







Actin filaments form a size-dependent diffusion barrier around centrosomes

Hsuan Cheng^{1,†} , Yu-Lin Kao^{1,†}, Ting Chen² , Lohitaksh Sharma¹, Wen-Ting Yang¹ , Yi-Chien Chuang¹, Shih-Han Huang¹, Hong-Rui Lin², Yao-Shen Huang¹, Chi-Ling Kao¹, Lee-Wei Yang^{2,3}, Rachel Bearon⁴, Hui-Chun Cheng² , Kuo-Chiang Hsia⁵  & Yu-Chun Lin^{1,6,*} 

Abstract

The centrosome, a non-membranous organelle, constrains various soluble molecules locally to execute its functions. As the centrosome is surrounded by various dense components, we hypothesized that it may be bordered by a putative diffusion barrier. After quantitatively measuring the trapping kinetics of soluble proteins of varying size at centrosomes by a chemically inducible diffusion trapping assay, we find that centrosomes are highly accessible to soluble molecules with a Stokes radius of less than 5.8 nm, whereas larger molecules rarely reach centrosomes, indicating the existence of a size-dependent diffusion barrier at centrosomes. The permeability of this barrier is tightly regulated by branched actin filaments outside of centrosomes and it decreases during anaphase when branched actin temporally increases. The actin-based diffusion barrier gates microtubule nucleation by interfering with γ -tubulin ring complex recruitment. We propose that actin filaments spatiotemporally constrain protein complexes at centrosomes in a size-dependent manner.

Keywords actin filaments; Centrosome; diffusion barrier; microtubule nucleation; γ -tubulin ring complex

Subject Categories Cell Adhesion, Polarity & Cytoskeleton; Cell Cycle

DOI 10.15252/embr.202254935 | Received 24 February 2022 | Revised 29

September 2022 | Accepted 11 October 2022 | Published online 31 October 2022

EMBO Reports (2023) 24: e54935

Introduction

Precise regulation of protein distribution and dynamics ensures proper cellular function and architecture, defects of which are associated with degenerative and neoplastic diseases (Aridor & Hanahan, 2000; Schaeffer *et al.*, 2014). Whereas active transport requires energy for molecules to move to their destination, soluble molecules

diffuse down a concentration gradient without energy expenditure in passive transport (Lin *et al.*, 2013b). To conduct local reactions, cells compartmentalize soluble molecules spatiotemporally by using diffusion barriers in various forms such as nuclear pore complexes, dendritic spine necks, axon initial segments, and ciliary pore complexes (Caudron & Barral, 2009; Nachury *et al.*, 2010; Hoelz *et al.*, 2011; Lin *et al.*, 2013b). These passive permeable diffusion barriers serve as conduits between different subcellular compartments and regulate the movement of soluble molecules across adjacent pools. Diffusion barrier deficiency results in protein mislocation/dissociation, which causes several known human diseases (Cronshaw & Matunis, 2004; Nachury *et al.*, 2010; Buffington & Rasband, 2011).

Eukaryotic cells contain endomembrane systems to compartmentalize molecules in membranous organelles for executing different functions (Rout & Field, 2017). Unlike most organelles, the centrosome is a non-membranous organelle; however, it is still capable of assembling hundreds of specific molecules locally and maintaining its microenvironment within the cytosol pool. These attributes ensure its proper architecture and function in terms of microtubule nucleation (Mahen & Venkitaraman, 2012; Chavali *et al.*, 2014) and formation of the primary cilium, an important protruding structure on the cell surface for sensing extracellular stimuli (Abal *et al.*, 2005; Bettencourt-Dias & Glover, 2007; Tang & Marshall, 2012; Chavali *et al.*, 2014). Many scaffold proteins serve as platforms to recruit centrosomal molecules from the cytosolic pool. Moreover, it is well known that the highly dense protein matrix that is present in confined areas is capable of forming permeable diffusion barriers (Westlake *et al.*, 2011). Based on the previous observation that centrosomes are embedded in a cloud of proteins known as the pericentriolar matrix, and emanating microtubules as well as branched actin filaments (Farina *et al.*, 2016; Strzyz, 2016), we hypothesized that a putative diffusion barrier may exist around centrosomes to constrain the distribution and dynamics of centrosomal molecules. To investigate the diffusion behavior of soluble molecules, several conventional approaches including single-particle tracking,

1 Institute of Molecular Medicine, National Tsing Hua University, Hsinchu, Taiwan

2 Institute of Bioinformatics and Structural Biology, National Tsing Hua University, Hsinchu, Taiwan

3 Physics Division, National Center for Theoretical Sciences, Taipei, Taiwan

4 Department of Mathematical Science, University of Liverpool, Liverpool, UK

5 Institute of Molecular Biology, Academia Sinica, Taipei, Taiwan

6 Department of Medical Science, National Tsing Hua University, Hsinchu, Taiwan

*Corresponding author. Tel: +886 35742421; E-mail: ycl@life.nthu.edu.tw

[†]These authors contributed equally to this work

fluorescence correlation spectroscopy, fluorescence recovery after photobleaching (FRAP), and tracking photoactivatable fluorescence proteins or microinjected molecules have been widely applied (Elowitz *et al*, 1997; Lukyanov *et al*, 2005; Venturoli & Rippe, 2005; Dertinger *et al*, 2007; Digman & Gratton, 2009; Hellriegel & Gratton, 2009; Zheng *et al*, 2011; Michalet & Berglund, 2012; Ries & Schwille, 2012; Lin *et al*, 2013a). However, the diffusion behaviors of molecules uncovered by these conventional methods are determined by both their intrinsic diffusion rates and extrinsic affinity for other immobile scaffolds, which cannot be easily uncoupled. To faithfully uncover the diffusion rates of soluble molecules independent of extrinsic interference, we applied a chemically inducible diffusion trap (CIDT), a previously developed approach, which permits the monitoring of molecule diffusion rates in specific subcellular sites while avoiding interactions between probes and immobile scaffolds in close proximity (Lin *et al*, 2013a, 2013b; Roll-Mecak, 2019). With the CIDT approach, we have identified a size-dependent diffusion barrier consisting of actin filaments as the key component around centrosomes.

Results

Establishment of centrosome-specific CIDT systems

We first describe how to use the CIDT approach to probe diffusion barriers. CIDT in living cells involves three components: rapamycin, a naturally occurring chemical dimerizer; FK506-rapamycin-binding domain (FRB); and immunophilin FK506-binding protein-12 (FKBP; DeRose *et al*, 2013). Introduction of rapamycin swiftly dimerizes FRB with nearby molecules of FKBP (Fig 1A; Banaszynski *et al*, 2005). Typically, FRB molecules are tagged with a known targeting sequence (TS in Fig 1A) and consequently anchored to regions of interest (ROIs), whereas FKBP molecules are tagged with diffusive probes (FKBP-probes) that uniformly distribute in the cytosolic pool. When the diffusive probes can access FRB-ROIs, the addition of rapamycin rapidly induces FRB/FKBP dimerization and consequently traps FKBP-probes from the cytosol onto FRB-ROIs (Fig 1A). In the presence of a diffusion barrier, however, the barrier can block certain FKBP-probes from the ROI (Fig 1A). In addition to accessibility, the trapping kinetics of FKBP-probes depend on their diffusion rates across cytosolic pools to FRB-ROIs. By measuring the kinetics of variably sized FKBP-probes that are trapped by FRB-ROIs, putative size-dependent diffusion barriers around FRB-ROIs can be characterized (Lin *et al*, 2013a, 2013b). CIDT has been successfully used to identify a size-dependent diffusion barrier at the base of the primary cilium (Lin *et al*, 2013a), which was also confirmed by other assays (Breslow *et al*, 2013).

To explore the putative diffusion barriers at centrosomes, we constrained FRB molecules at centrosomes by tagging FRB with centrosome-targeting sequences (CTSs; Fig 1B). It is necessary to select CTSs with low shuttling and highly sustained localization at the designated centrosomal sub-compartments in an attempt to focus on probe diffusion and avoid interference from the active transport of probes, as would be facilitated by CTSs that are highly mobile. Therefore, we took advantage of the FRAP assay to explore and evaluate the dynamics of several previously identified CTS candidates including CEP120C (C terminus of CEP120, which localizes

at the centriolar outer wall; Mahjoub *et al*, 2010), CEP170C (C terminus of CEP170, which localizes at subdistal appendages; Higgs & Peterson, 2005), PACT (C terminus of Pericentrin, which localizes at the pericentriolar matrix), Centrin2 (which localizes to the centriolar lumen; Paoletti *et al*, 1996), and PCM1F2 (F2 domain of PCM1, which localizes at centriolar satellites; Wang *et al*, 2013). Among these, green fluorescent protein (GFP)-tagged CEP120C and CEP170C showed the most rapid recovery after photobleaching (Fig EV1A–C) with high mobile fractions (> 20%) and low recovery half-time (< 60 s; Fig EV1C), indicating constant centrosome cytoplasmic shuttling of CEP120C and CEP170C. Meanwhile, PCM1F2, PACT, and Centrin2 were capable of constraining a cyan fluorescent protein, Cerulean3 (Ce3), and the FRB molecule in specific sub-compartments of centrosomes (Ce3-FRB-Centrin2 at centriolar lumen; PACT-Ce3-FRB at pericentriolar matrix; PCM1F2-Ce3-FRB at centriolar satellites; Fig EV2), show a low shuttling rate with a low mobile fraction (< 20% in 5 min; Fig EV1B and C), making them suitable CTSs for the CIDT system.

We confirmed that rapamycin treatment triggers the trapping of cytosolic FKBP-tagged probes in the ROIs where the corresponding CTS-FRB proteins reside by co-expressing yellow fluorescent protein (YFP)-tagged FKBP (YFP-FKBP; Stokes radius [Rs], 3.2 nm; molecular weight, 40 kDa) with PCM1F2-Ce3-FRB, PACT-Ce3-FRB, and Ce3-FRB-Centrin2 in U2Os cells, a cell type derived from human osteosarcoma that exhibits clear centrosomal structures (Fig 2A; Movies EV1–EV3, left). The accumulation of YFP-FKBP onto each centrosome locale quickly reached a plateau level, probably due to the full occupancy of FRB-binding sites locally (Fig 2B). The half-time ($t_{1/2}$) values for translocation of YFP-FKBP onto three probe-targeted sites were all similar (Centrin2: 12.15 ± 2.27 s; PACT: 13.83 ± 3.09 s; PCM1F2: 7.24 ± 0.46 s). This confirmed the applicability of the centrosome CIDT method in our subsequent experiments.

Recruiting varisized diffusion probes onto centrosomes

We investigated the diffusion of varisized proteins at three centrosome locales in U2Os cells. Native Rs (Stokes radius) for YFP-FKBP, YFP-FKBP-Grp1, YFP-FKBP-Luciferase, YFP-PSD95-FKBP, YFP-FKBP- β -Gals, YFP-FKBP- β -Galm, YFP-FKBP- Δ N β -Gal, and YFP-FKBP- β -Gal were 3.2, 4.1, 4.5, 5.2, 5.8, 6.0, 6.3, and 7.6 nm, with molecular weights of 40, 57, 100, 122, 230, 262, 322, and 659 kDa, respectively, according to previous study and measurement of size exclusion chromatography in the present study (Table EV1; details in Materials and Methods; Lin *et al*, 2013a). Western blot analysis confirmed that full-length probes can be detected as major bands in expected molecular weight (Appendix Fig S1). One exception that YFP-FKBP-Luciferase displayed few degraded forms in lower molecular weight (Appendix Fig S1), probably due to previously reported proteolytic degradation (Ataei *et al*, 2009). Based on the size measurement using size exclusion chromatography, full-length β -Gal and three truncated β -Gal proteins form hexamer (YFP-FKBP- β -Gal: 659 kDa) and dimer (YFP-FKBP- β -Gals: 230 kDa; YFP-FKBP- β -Galm: 262 kDa; YFP-FKBP- Δ N β -Gal: 322 kDa), respectively.

We next co-expressed PCM1F2-Ce3-FRB and each of the YFP-FKBP-tagged probes in U2Os cells. All varisized diffusion probes immediately translocated onto the centrosome peripheral,

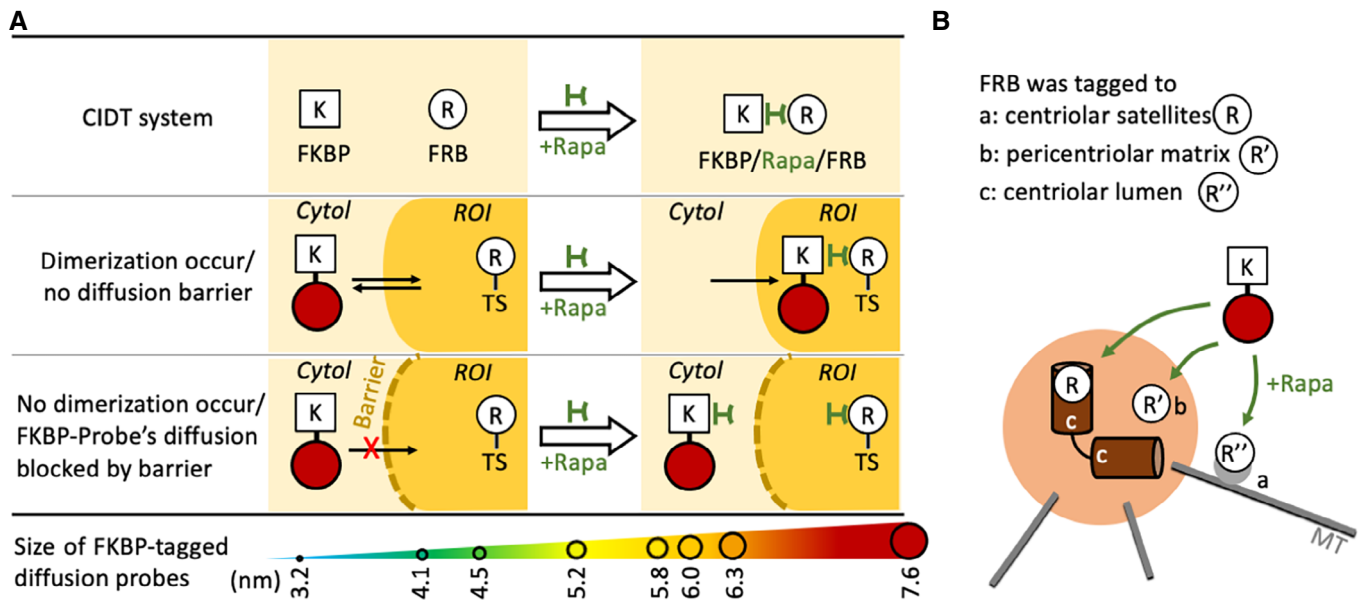


Figure 1. Using the CIDT system to probe a putative centrosomal diffusion barrier.

A With the CIDT (chemically inducible diffusion trapping) system, YFP-FKBP-tagged diffusive protein probes (FKBP-probes) ranging from 40 to 659 kDa (3.2–7.6 nm) were used to probe the putative diffusion barrier in cells. FRB was localized to region of interest (ROI) by tagging with the targeting sequence of ROI (TS). Theoretically, in the absence of a barrier (middle panel), probes can freely access and be trapped at ROI via rapamycin (Rapa)-triggered FRB/FKBP dimerization; in the presence of a barrier (lower panel), probe diffusion can be hindered and, thus, dimerization obstructed.

B To explore the precise location of putative diffusion barriers at centrosomes, FRB (R) was tagged to localize to three different sub-compartments of centrosomes, the centriolar satellites (a), pericentriolar matrix (b), and centriolar lumen (c). The accessibilities of FKBP (K)-tagged diffusion probes of various sizes to centrosomes were tested by the CIDT system.

PCM1F2-labeled centriolar satellites, upon rapamycin treatment (Fig 3A and B, left; Appendix Figs S2–S9 and Movie EV1). Interestingly, whereas probes with an Rs as large as 5.8 nm still showed rapid translocation onto all three centrosomal sub-compartments, YFP-FKBP- β -Gals (6.0 nm) and two larger probes (YFP-FKBP- Δ N β -Gal: 6.3 nm and YFP-FKBP- β -Gal: 7.6 nm) rarely or cannot translocate onto the pericentriolar matrix and centriolar lumen, within 4 min upon rapamycin treatment (Fig 3A and B, middle and right panels; Appendix Figs S2–S9 and Movies EV2 and EV3). We further evaluated the binding between CTS-Ce3-FRB and two large probes (YFP-FKBP- Δ N β -Gal and YFP-FKBP- β -Gal) by FRET (fluorescence resonance energy transfer), a process that transfers energy from Ce3 to YFP once they associate with each other. Although YFP-FKBP- Δ N β -Gal and YFP-FKBP- β -Gal cannot be trapped at PACT and Centrin2-labeled centrosome regions, a weak FRET signal can be observed in cytosol upon rapamycin treatment (Fig EV3A–D). As expected, these large probes generated strong FRET signal with cytosolic Ce3-FRB in cytosol right after rapamycin treatment. Altogether, these results confirmed that YFP-FKBP- Δ N β -Gal and YFP-FKBP- β -Gal are able to bind to target sequence-tagged FRB molecules in cytosolic pool while this binding does not occur at centrosomes, suggesting their poor diffusivities to centrosomes.

We further quantified the translocation probability by extending the translocation time to 2 h after trapping the diffusive probes by rapamycin treatment. Cells transfected with 24 combinations of one CFP-FRB-ROI and one YFP-FKBP-tagged probe representing each condition were treated with rapamycin for 2 h (Table EV1). The probability of trapping each probe in centriolar satellites are all over

90% (Table EV1). Small probes (≤ 5.8 nm) can fully access the pericentriolar matrix and centriolar lumen (Table EV1). However, the probabilities of trapping bigger probes (≥ 6.0 nm) to pericentriolar matrix and centriolar lumen gradually decline as protein size increases (Table EV1). In conclusion, the diffusion of soluble proteins ranging from an Rs of 3.2 to 7.6 nm (40–659 kDa) at centriolar satellites was similar, whereas their diffusion/accumulation at the PACT-tagged pericentriolar matrix and Centrin2-tagged centriolar lumen showed a negative correlation. The probability of accessing peripheral centriolar satellites for soluble diffusive probes with Rs ≥ 6.0 nm (262 kDa) is still high but plummets at the pericentriolar matrix and centriolar lumen. The poor diffusivities of large probes at the centrosome core are not determined by their diffusivities in the cytosol, as the trapping kinetics of those probes to centriolar satellites and to the plasma membrane are all rapid (Figs 3 and EV4A and B; Movie EV1). Given that the rapid recruitment occurred within a minute, the mTOR pathway was not likely to contribute to the diffusive effect despite the addition of rapamycin. Taken together, these results revealed the existence of a size-dependent diffusion barrier between the core centrosomes and cytosol pool.

Actin filaments contribute to the centrosomal diffusion barrier

We next aimed to explore the molecular components of the centrosomal diffusion barriers. Centrosomes are known to be microtubule- and actin-organizing centers that are surrounded by these cytoskeletal elements (Mahen & Venkitaraman, 2012; Pihan, 2013; Chavali et al, 2014; Farina et al, 2016; Obino

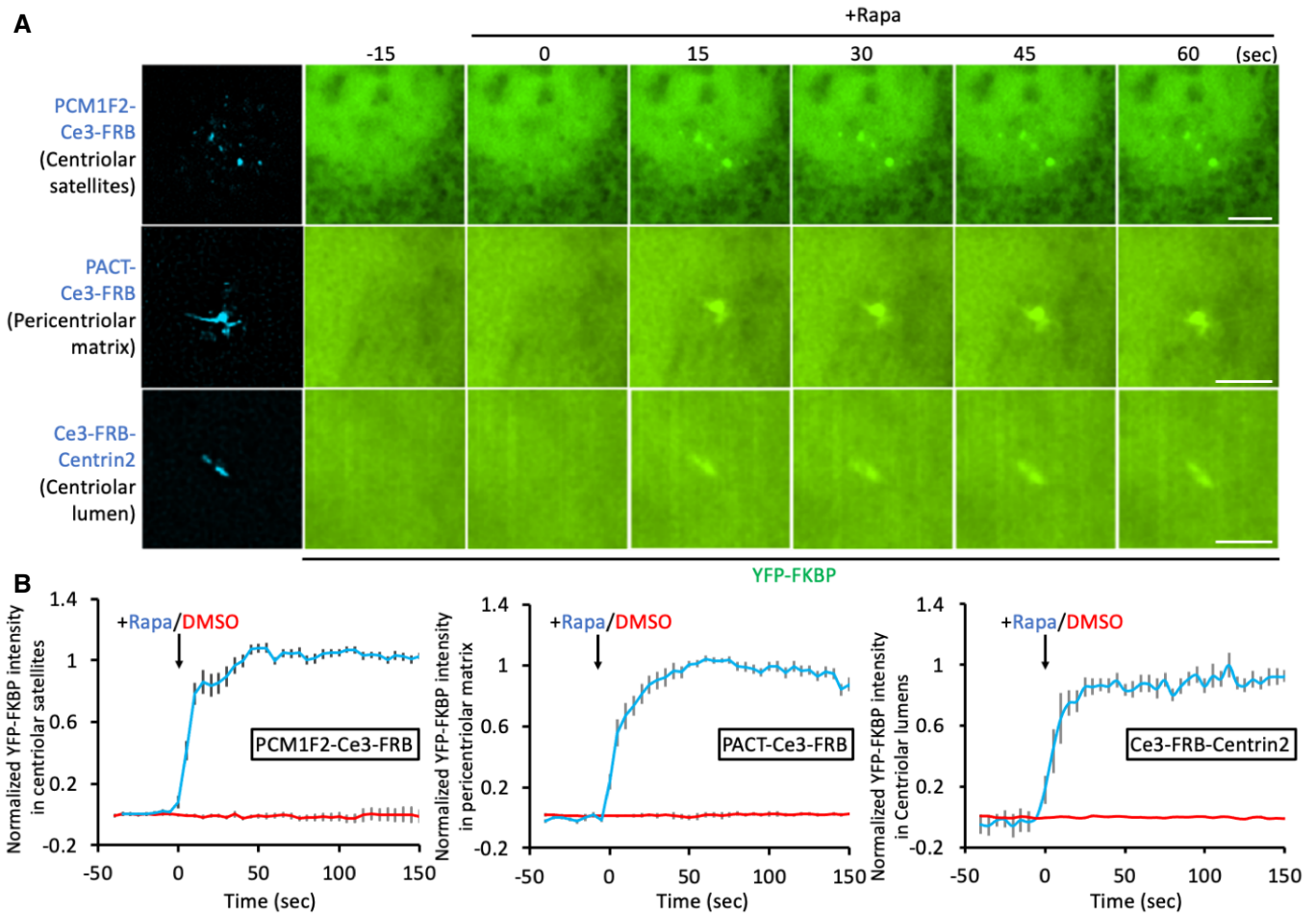


Figure 2. Trapping diffusion probes at three centrosomal sub-compartments.

A U2Os cells co-transfected with YFP-FKBP and PCM1F2-Ce3-FRB, PACT-Ce3-FRB, or Ce3-FRB-Centrin2 were treated with rapamycin (100 nM). The translocation of YFP-FKBP onto PCM1F2-Ce3-FRB-labeled centriolar satellites, the PACT-Ce3-FRB-labeled pericentriolar matrix, and the Ce3-FRB-Centrin2-labeled centriolar lumen was monitored. Scale bars, 5 μ m.

B The normalized fluorescence intensity of YFP-FKBP accumulation at centrosomes upon rapamycin (100 nM; blue) and DMSO (0.1%, vehicle control; red) treatment. Data are shown as the mean \pm SEM. The graphs show immediate translocation of YFP-FKBP after rapamycin induction at centriolar satellites (left, $n = 24$ cells), the pericentriolar matrix (middle, $n = 20$ cells), and the centriolar lumen (right, $n = 23$ cells) from seven independent experiments.

et al., 2016). We hypothesized that either microtubules or actin filaments contribute to the function and composition of centrosomal diffusion barriers, as it is known that the cytoskeleton not only provides mechanical support but also serves as a critical component of permeable passive barriers in cells (Potma *et al.*, 2001).

To examine the role of microtubules in centrosomal diffusion barriers, U2Os cells were treated with Nocodazole to depolymerize the cellular microtubule polymers to soluble tubulins (Musa *et al.*, 2003). An immunostaining assay confirmed that microtubule depolymerization occurred 20 min after Nocodazole treatment (Figs 4A and B, and EV5A and B). Moreover, dispersed centriolar satellites were observed in Nocodazole-treated cells, indicating that microtubules are fully depolymerized (Fig EV5C and D). We then carried out the CIDT assay on cells with either intact or depolymerized microtubules. Our results showed that YFP-FKBP- Δ N β -Gal was blocked from entering Centrin2-tagged centriolar lumen or

pericentriolar matrix even after microtubule depolymerization. While no difference is observed in accessibilities during trapping of different probes to centrosome post-microtubule impairment (Fig 4C and D), these results indicate that the contribution of microtubules with respect to the diffusion barrier was rather trivial.

We next investigated the role of actin filaments. Centrosomes are surrounded by Arp2/3-associated branched actin filaments (Wu *et al.*, 2018). We disrupted actin filaments in U2Os cells by the addition of CK666, an Arp2/3 inhibitor (Yang *et al.*, 2012; Hetrick *et al.*, 2014), and Latrunculin A, which perturbs actin polymerization (Nolen *et al.*, 2009; Fujiwara *et al.*, 2018; Inoue *et al.*, 2019). Immunofluorescence results showed that CK666 and Latrunculin A reduced ~ 60.11 and $\sim 30.59\%$ of centrosomal actin, respectively (Fig 4E and F). A CIDT assay in the presence of CK666 showed that the decrease in centrosomal actin filaments allowed the entry of YFP-FKBP- Δ N β -Gal and YFP-FKBP- β -Gal, which could not access

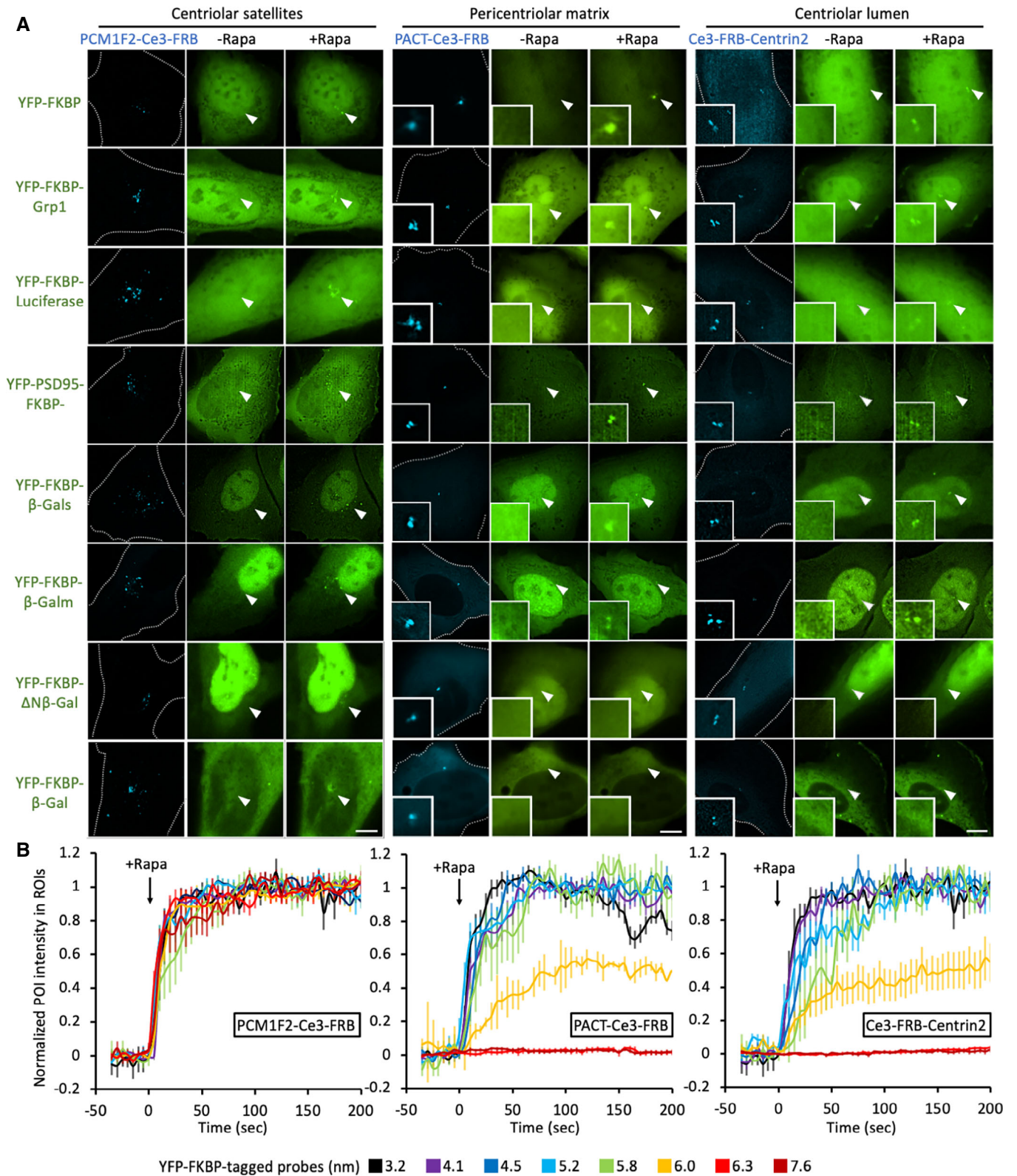


Figure 3.

Figure 3. Size-dependent accessibility of diffusion probes into centrosomes.

- A U2Os cells co-transfected with each YFP-FKBP-labeled varized probe (YFP-FKBP, YFP-FKBP-Grp1, YFP-FKBP-Luciferase, YFP-PSD95-FKBP, YFP-FKBP- β -Gals, YFP-FKBP- β -Galm, YFP-FKBP- Δ N β -Gal, and YFP-FKBP- β -Gal) and Ce3-FRB with labels specific for centrosomal sub-compartments were treated with rapamycin (100 nM). The images of cerulean channel show centrosome sub-compartment from the untreated cells. Arrowheads indicate sites of centrosomes. Insets show higher-magnification images of the centrosomal regions. Dotted lines indicate the cell boundaries. Scale bars, 10 μ m.
- B The normalized fluorescence intensity of each probe at centriolar satellites (left, $n = 14, 19, 17, 13, 11, 22, 14,$ and 9 cells from small to large probes), pericentriolar matrix (middle, $n = 20, 19, 18, 16, 10, 18, 10,$ and 12 cells from small to large probes), and centriolar lumen (right, $n = 10, 13, 13, 6, 3, 19, 13,$ and 9 cells from small to large probes) from three to six independent experiments. Data are shown as the mean \pm SEM.

the centriolar lumen and pericentriolar matrix in the absence of CK666 (Fig 4G and H). Perhaps due to the modest effect of actin disruption triggered by Latrunculin A (Fig 4F), only YFP-FKBP- Δ N β -Gal but not YFP-FKBP- β -Gal can be trapped to centrosomes after Latrunculin A treatment (Fig 4H). A higher concentration of Latrunculin A (1 mM) caused cell shrinkage and therefore was excluded. The amount of centrosomal actin filaments is inversely correlated to centrosome accessibility. ~ 39.89 and $\sim 69.41\%$ actin was left around centrosomes upon CK666 and Latrunculin A treatment, making centrosomes accessible to 7.6 nm and 6.3 nm probes, respectively (Fig 4F and H). Nevertheless, these results indicate the substantial contribution of actin filaments to the composition of the centrosomal size-dependent diffusion barrier.

Previous studies showed a reciprocal relationship between microtubules and branched actin level around centrosomes (Farina *et al.*, 2019; Inoue *et al.*, 2019), raising a possibility that Nocodazole-mediated microtubule depolymerization may increase branched actin filaments around centrosomes. To address this, we measured the level of centrosomal actin filaments after Nocodazole treatment. Surprisingly, there was a slight reduce ($\sim 20\%$) in centrosomal actin filaments post-Nocodazole treatment (Fig EV5E and F). This is probably because Nocodazole treatment inhibits dynein and slightly reduces the level of Arp2/3 complex at centrosomes, a mechanism for Arp2/3 recruitment at centrosomes that has been reported before (Farina *et al.*, 2016). Such a modest effect of actin disruption indirectly triggered by Nocodazole does not affect centrosome accessibility (Fig 4C and D).

The permeability of centrosomal diffusion barriers decreases in anaphase

At anaphase, an increase in the amount of branched actin filaments around centrosomes was observed (Farina *et al.*, 2019). We therefore tried to characterize the permeability of centrosomal diffusion barriers in anaphase cells. Sequential treatment of thymidine and RO3306 was used to synchronize cells at G2/M phase (Appendix Fig S10A–C). A total of 45–60 min after RO3306 removal, anaphase cells were identified based on H2B-RFP-labeled chromosomes and applied to probe trapping experiments (Fig 5A). In interphase HeLa cells, YFP-FKBP-Luciferase (4.5 nm) could access PACT-labeled pericentriolar matrix (Fig 5A and B). However, the entry of YFP-FKBP-Luciferase onto centrosomes was blocked in anaphase cells (Fig 5A and B). Moreover, the probabilities of trapping YFP-FKBP-Luciferase (4.5 nm) and YFP-FKBP- Δ N β -Gal (6.3 nm) to anaphase centrosomes were significantly less than that in interphase cells (Fig 5C). We confirmed that the permeability of centrosomal diffusion barriers temporally decreased during anaphase. To test whether branched actin filaments are required for

centrosomal diffusion barriers during anaphase, transfected cells were synchronized and pretreated with CK666, followed by trapping experiments. CK666 treatment significantly increased the probability of YFP-FKBP-Luciferase (4.5 nm) trapping to centrosomes in anaphase (Fig 5D and E), confirming that branched actin filaments are important for centrosomal diffusion barrier.

The actin-based diffusion barrier physically regulates γ -TuRC and microtubule nucleation

The centrosome acts as a microtubule-organizing center via recruiting the γ -tubulin ring complex (γ -TuRC), a key protein complex (Rs: ~ 15 nm; Oegema *et al.*, 1999) required for microtubule nucleation, onto centrosomes (Wu & Akhmanova, 2017). We tried to examine whether the centrosome diffusion barrier gates the recruitment of γ -TuRC at centrosomes. The density of one major component in γ -TuRC, γ -tubulin, in control and CK666-treated centrosomes was labeled and quantified. Disruption of actin-based diffusion barriers significantly increased the amount of γ -tubulin at centrosomes (Fig 6A and B). It is known that γ -TuRC is essentially assembled by proteins of GCP (Gamma tubulin complex protein) family and γ -tubulin (Haren *et al.*, 2020; Thawani & Petry, 2021). As GCP4 (Gamma-tubulin complex component 4) is an essential molecule for γ -TuRC assembly, we carefully tested the feasibility of using GFP-tagged GCP4 as a marker of γ -TuRC in live-cell imaging. Fluorescence images showed that GFP-tagged full-length GCP4 presents as puncta and highly colocalizes with γ -tubulin (Appendix Fig S11A). However, GCP4 Δ C, a truncated GCP4 protein that cannot associate with γ -TuRC based on fractionation data (Farache *et al.*, 2016), mainly located in cytosol and did not or rarely show the GCP4⁺/ γ -tubulin⁺ foci in cells (Appendix Fig S11A and B). Altogether, these results suggest that full-length GCP4-positive foci can serve as a marker of γ -TuRC for further evaluating its distribution and dynamics in cells.

With this γ -TuRC marker, the FRAP assay was used to evaluate the centrosome accessibility for γ -TuRC (GCP4-GFP-positive foci) in control and CK666-treated centrosomes (Fig 6C; Movie EV4). After disruption of branched actin, the recovery rate of GCP4-GFP was faster compared with control cells (Fig 6D). The higher mobile fraction and shorter recovery half-time of GCP4-GFP in CK666-treated centrosomes (Fig 6D) suggesting that recruitment of γ -TuRC is constrained by centrosome branched actin. We next transfected U2Os cells with EB1-mNeon, a microtubule plus-end marker tagged with a green/yellow fluorescent protein, mNeon, to track microtubule growth (25 μ m in diameter) in the cells with either an intact or disrupted (CK666 treated) diffusion barrier (Fig 6E). We quantitatively measured the frequency of microtubule nucleation and the microtubule elongation rate, events indicative of microtubule

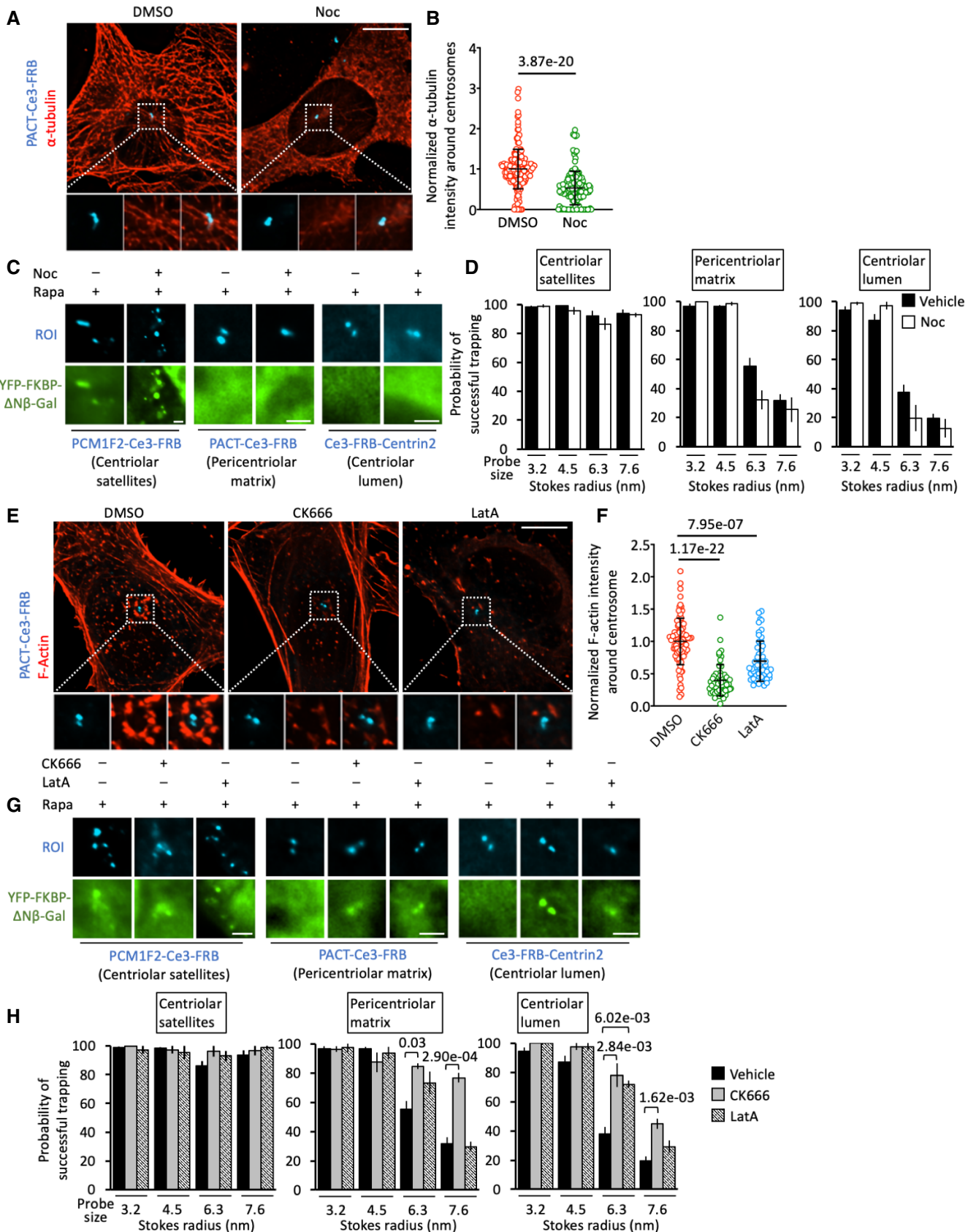


Figure 4.

Figure 4. Branched actin filaments are key components of centrosomal diffusion barriers.

- A Depolymerization of microtubules by Nocodazole (10 μ M) treatment. U2Os cells that expressed PACT-Ce3-FRB (blue, a marker of centrosomes) were incubated with antibodies against α -tubulin to label microtubules (red) in the absence (0.1% DMSO) or presence of Nocodazole treatment for 20 min. Lower panels show magnified images of the centrosomal regions. Scale bar, 10 μ m.
- B The normalized intensity of α -tubulin around centrosomes in the absence or presence of Nocodazole treatment for 20 min. The circular ROIs in diameter of 3 μ m, centering PACT-labeled centrosomes, were used for measurement of the level of microtubule around centrosomes. Data (black) are shown as the mean \pm SD. (n = 196 and 156 cells from left to right; three independent experiments).
- C U2Os cells co-transfected with the indicated constructs were treated with rapamycin (Rapa, 100 nM) in the absence or presence of 20-min Nocodazole pretreatment. Scale bar, 2 μ m.
- D The percentage of vehicle (DMSO)- or Nocodazole-treated cells exhibiting probe translocation. 1,205, 246, 1,291, 235, 1,010, and 227 cells in centriolar lumen-vehicle, centriolar lumen-Nocodazole, pericentriolar matrix-vehicle, pericentriolar matrix-Nocodazole, centriolar satellites-vehicle, and centriolar satellites-Nocodazole groups, respectively, from three to 12 independent experiments were analyzed. Data are shown as mean \pm SEM.
- E U2Os cells expressing PACT-Ce3-FRB (blue, a marker of centrosomes) were incubated with phalloidin to label the F-actin (red) with DMSO (0.1%), CK666 (0.4 mM) for 2 h, or Latrunculin A (LatA, 0.5 mM) for 1 h. Lower panels show the magnified images of the centrosomal regions. Scale bar, 10 μ m.
- F The normalized intensity of actin filaments around centrosomes in the absence or presence of CK666 or LatA treatment. The circular ROIs in diameter of 3 μ m, centering PACT-labeled centrosomes, were used for measurement of the level of actin filaments around centrosomes. Data (black) are shown as the mean \pm SD. (n = 85, 55, and 55 cells from left to right; 3 independent experiments).
- G U2Os cells co-transfected with the indicated constructs were treated with rapamycin (Rapa, 100 nM) in the absence or presence of 2 h-CK666 or 1 h-LatA pretreatment. Scale bar, 2 μ m.
- H The percentage of vehicle (DMSO)-, CK666- or LatA-treated cells exhibiting probe translocation onto centrosomes (1,205, 245, 194, 1,291, 288, 219, 1,010, 165, and 48 cells in centriolar lumen-vehicle), centriolar lumen-CK666, centriolar lumen-LatA, pericentriolar matrix-vehicle, pericentriolar matrix-CK666, pericentriolar matrix-LatA, centriolar satellites-vehicle, centriolar satellites-CK666, and centriolar satellites-LatA groups, respectively, from three to 12 independent experiments were analyzed. Data are shown as mean \pm SEM.

Data information: Student's *t*-tests were performed with *P* values indicated. (*P* values larger than 0.05 are not shown).

growth in the centrosome core region and in the cytosol, respectively. The number of nascent microtubules derived from centrosomes was significantly increased in the absence of a diffusion barrier as compared with that in control cells (Fig 6F). Disruption of the diffusion barrier did not, however, affect the elongation rate of microtubules in cytosol (Fig 6G). These results suggest that recruitment of γ -TuRC and initiation of microtubule growth around centrosomes were hindered by the diffusion barrier, whereas their elongation rate was not perturbed after they had elongated away from the centrosomes.

Discussion

We here established a centrosome-specific CIDT system that enables rapid recruitment of varisized cytosolic diffusive probes to three centrosome locales, ranging from the core to the periphery. Diffusive probes with an *R*_s of \leq 5.8 nm (230 kDa) can freely access all centrosome sub-compartments, whereas the accessibility of large diffusive probes was hindered. Probes with an *R*_s of \geq 6.0 nm

(262 kDa) rarely or cannot reach the pericentriolar matrix and centriolar lumen, indicating the existence of a size-dependent diffusion barrier outside the centrosomal core region. The centrosomal diffusion barrier was perturbed after disruption of branched actin filaments. Disruption of the centrosomal diffusion barrier enabled the entry of large molecules and γ -TuRC as well as increased microtubule nucleation. The permeability of actin-based barriers was temporally decreased in anaphase. In summary, these results suggest that actin-based diffusion barriers outside of centrosomes spatiotemporally gate the diffusion of molecules in a size-dependent manner.

According to our CIDT results, cytosolic molecules with an *R*_s of \leq 5.8 nm can freely access centrosomal core regions. Therefore, most cytosolic components, such as small proteins, metabolites, ions, mRNAs, and others, are able to reach the interior of centrosomes. Intuitively, anchoring via their affinity for centrosomal scaffold proteins should be the major mechanism by which small molecules are retained at centrosomes for local reactions. Conversely, without active transport mediated by motor proteins, large molecules (*R*_s \geq 6.0 nm; 262 kDa) such as protein complexes,

Figure 5. The permeability of centrosomal diffusion barriers decreases in anaphase.

- A HeLa cells co-transfected with H2B-RFP (a chromosome marker), PACT-Ce3-FRB, and YFP-FKBP-Luciferase were sequentially incubated with thymidine (2 mM) for 16–18 h and RO3306 (2.5 ng/ml) for 12 h to synchronize cells in G2/M phase (Interphase cells in left panel). The probe trapping experiment in interphase cells was performed right after RO3306 washout. Anaphase cells were chosen for probe trapping experiment 45–60 min after RO3306 washout. Transfected cells in interphase or anaphase were treated with 100 nM rapamycin (Rapa). The centrosome regions are shown in lower panels. Scale bar, 10 μ m.
- B The normalized fluorescence intensity of YFP-FKBP-Luciferase accumulation at centrosomes in interphase (Green, n = 12 cells) or anaphase (Red, n = 10 cells) cells upon rapamycin (100 nM) treatment. Data are shown as the mean \pm SEM.
- C The percentage of interphase or anaphase cells exhibiting probe translocation. Data are shown as mean \pm SEM. (n = 187, 46, 120, 28, 102, 82, 132, and 29 cells from left to right, respectively; three independent experiments).
- D HeLa cells co-transfected with H2B-RFP (a chromosome marker), PACT-Ce3-FRB, and YFP-FKBP-Luciferase were synchronized in anaphase with or without CK666 treatment (0.4 mM). Rapamycin (100 nM) was added for 5 min to trigger the YFP-FKBP-Luciferase trapping at centrosomes. The right panel is the enlarged images of centrosome regions and arrows indicated centrosome sites. Scale bar, 10 μ m.
- E The percentage of cells in D exhibiting probe translocation. Data are shown as mean \pm SEM. (n = 47 and 31 cells in DMSO- and CK666-treated groups, respectively; three to four independent experiments).

Data information: Student's *t*-tests were performed with *P* values indicated. *P* values larger than 0.05 are not shown.

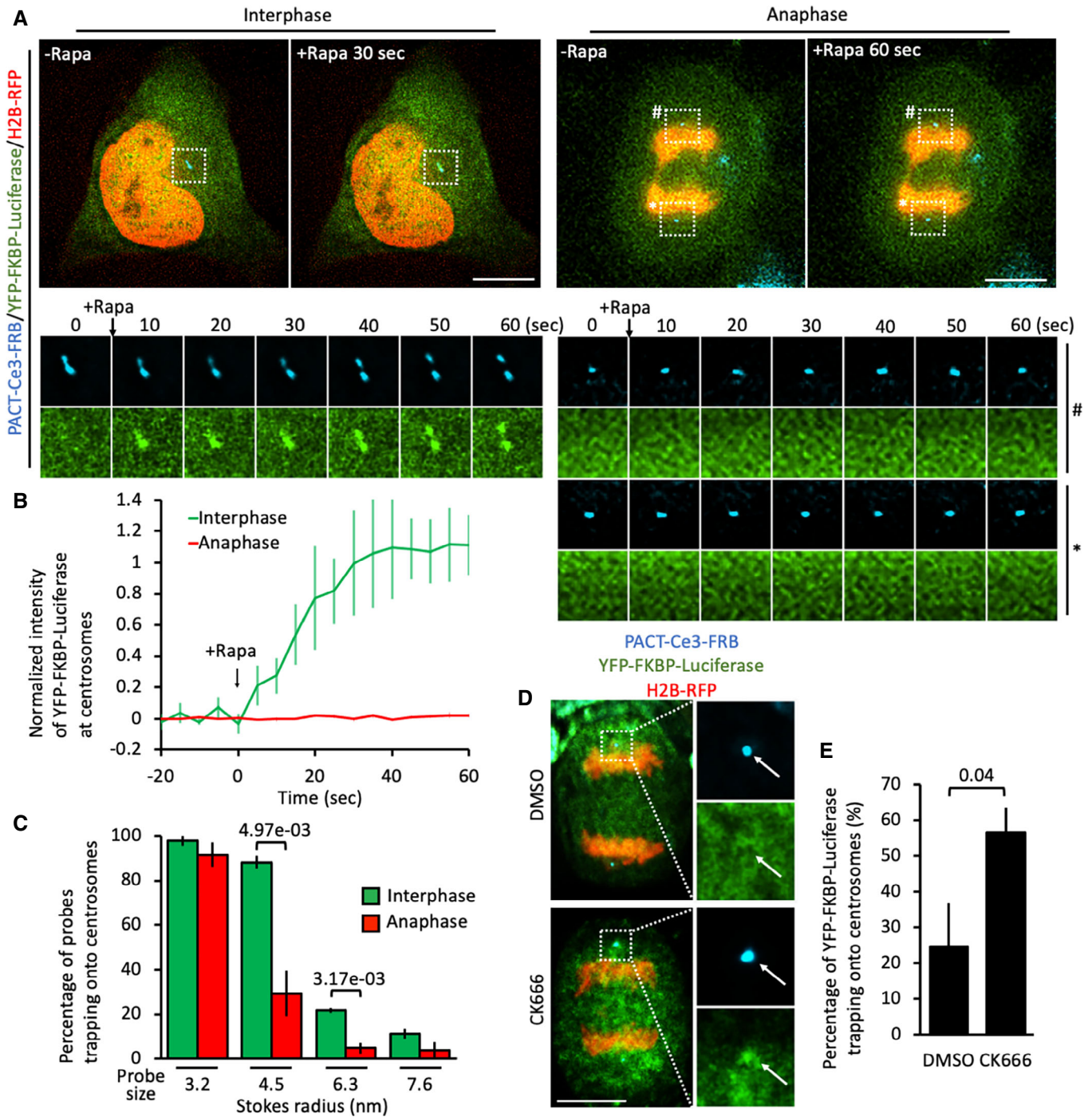


Figure 5.

aggresomes, and ribosomes are prohibited from centrosomes. For example, proteasomes are soluble protein complexes that locally trigger proteolytic degradation at centrosomes (Kopito, 2000). Because of their very large size (20 S proteasome: ~ 750 kDa; Tanahasi et al, 1993), we assume that proteasomes cannot access centrosomal core region to directly trigger protein degradation.

Alternatively, centrosomal proteins may diffuse to the cytosol pool that is proximal to centrosomes for proteasome-mediated degradation. Indeed, excess centrosomal proteins and misfolded proteins accumulate in regions proximal to centrosomes upon inhibition of proteasome activity, which supports our assumption (Johnston et al, 1998; Kopito, 2000).

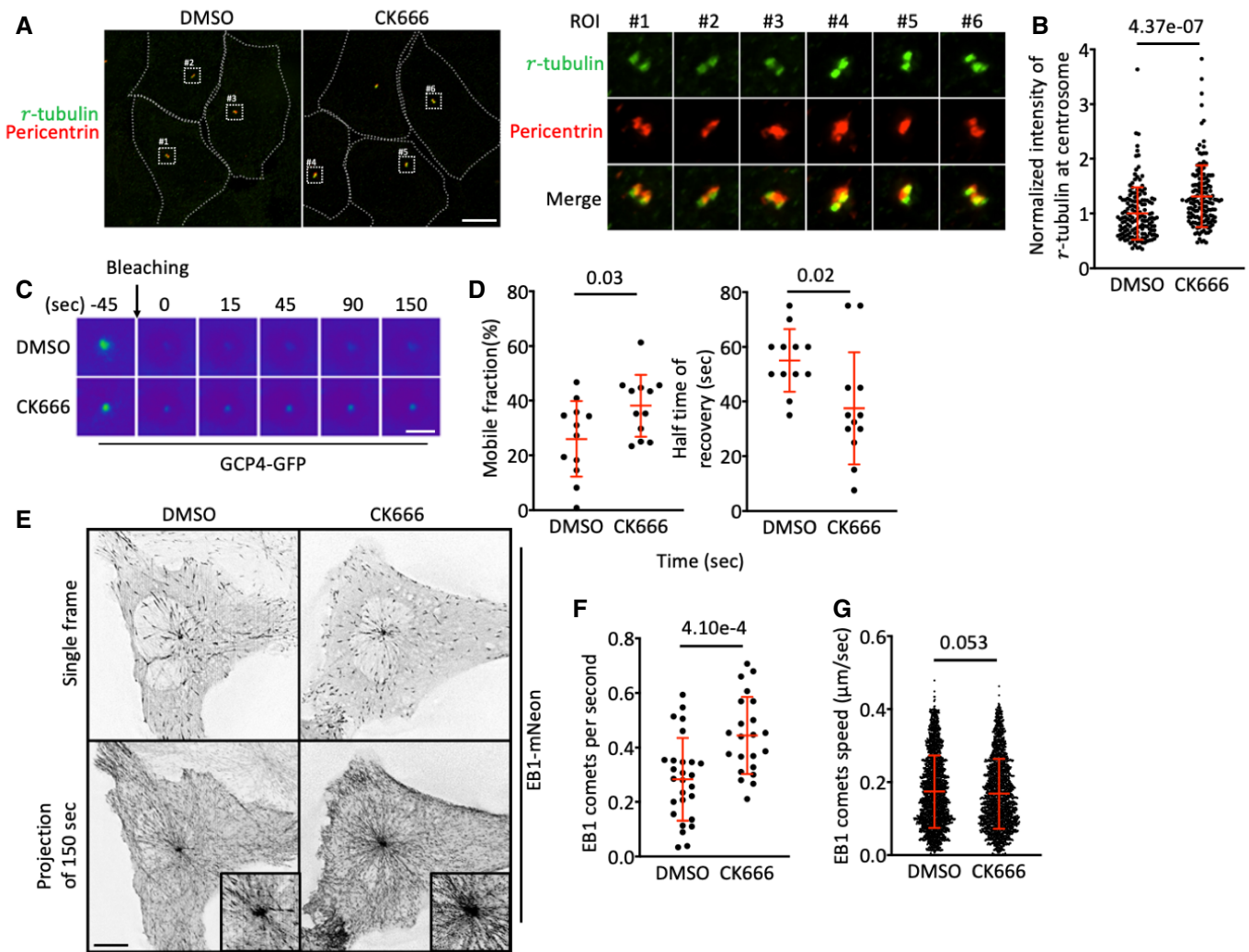


Figure 6. Centrosomal diffusion barriers constrain γ -TuRC recruitment and microtubule nucleation.

- A** U2Os cells were incubated with antibodies against γ -tubulin (green; a marker of γ -TuRC) or Pericentrin (red; a marker of centrosomes) in the absence (0.1% DMSO) or presence of CK666 treatment (0.4 mM) for 2 h. The right panel shows magnified images of the indicated region of interest (ROI). Scale bar, 10 μm .
- B** The normalized intensity of γ -tubulin at centrosome in control (0.1% DMSO, 2 h) or CK666 (0.4 mM, 2 h)-treated cells. Individual data points and the mean \pm SD. (in red) are shown ($n = 150$ and 150 cells in DMSO- and CK666-treated group, respectively; four independent experiments).
- C** U2Os cells transfected with GCP4-GFP were treated with or without CK666 (0.4 mM, 2 h) and then observed for the indicated time after photobleaching. Scale bar, 5 μm .
- D** The mobile fraction percentage (left) and mobile recovery half-time (right) of GCP4-GFP in FRAP experiments (C). Data (red) are shown as mean \pm SD. $n = 12$ and 12 cells in DMSO- and CK666-treated group, respectively; three independent experiments.
- E** U2Os cells expressing EB1-mNeon were incubated with 0.1% DMSO or 0.4 mM CK666 for 2 h. Images were captured over 150 s and were overlaid to show the overall tracks of the microtubules. The insets show enlarged images of the centrosomal regions. Scale bar, 10 μm .
- F, G** The number of microtubule tracks that emanate from centrosomes (F) and the microtubule elongation rate (G) in the absence and presence of CK666 treatment (0.4 mM). Individual data points and the mean \pm SD. (in red) are shown ($n = 78,449$ and 54,283 microtubule tracks from 27 and 22 cells in the DMSO- and CK666-treated groups, respectively; three independent experiments).

Data information: Student's *t*-tests were performed with *P* values indicated.

We demonstrated that branched actin filaments, also abundant in dendritic spines, the axon initial segment, and other subcellular regions (Song *et al*, 2009; Balasanyan *et al*, 2017; Turner-Bridger *et al*, 2018), act as a diffusion barrier around centrosomes. Not surprisingly, the dense actin meshwork in these sites also functions as a diffusion barrier. Actin filaments in dendritic spines restrict the mobility of proteins larger than 100 kDa. This restriction is reduced

during actin reformation in structural plasticity or after actin filaments are severed by latrunculin A (Fujiwara *et al*, 2018). The actin-based diffusion barrier in axonal initial segments ensures axon integrity and neuron cell polarity by preventing dendritic protein-positive vesicles from accessing the axonal lumen (Balasanyan *et al*, 2017). Consistent with the study that shows distribution of actin patches, without complete coverage, at axon initial segment

block the diffusion of 70 kDa probe (Song *et al*, 2009; Turner-Bridger *et al*, 2018), we found that centrosomes are surrounded by actin patches with few gaps (Fig 4E) which spatially hinder the entry of probes ≥ 262 kD. Whether other actin-associated molecules compose network functioning as a barrier is worthy of studying in the future. As centrosomes are transformed into basal bodies at the entrance to the lumen of the primary cilium during G0 phase, we assumed that centrosomal diffusion barriers may also halt the entry of cytosolic molecules into the ciliary lumen. However, previous studies demonstrated that proteins with an Rs as large as 7.9 nm can access the ciliary lumen (Breslow *et al*, 2013; Lin *et al*, 2013a). One possible explanation for this is that centrosomal diffusion barriers do not span the entire ciliary base. Ultrastructural observations of branched actin filaments and the ciliary base are needed to confirm this assumption.

Actin cytoskeleton homeostasis is spatiotemporally regulated by assembly factors such as Arp2/3 complex and formins, two mechanisms assembling short-branched F-actin networks and long-unbranched F-actin, respectively (Burke *et al*, 2014). Moreover, these two assembly pathways compete for a limited pool of actin monomers (Burke *et al*, 2014). Inhibition of Arp2/3-dependent branched actin therefore causes an increased formation of long-unbranched F-actin in cells. However, previous studies demonstrated that branched actin meshwork but not unbranched actin bundles hinder microtubule growth in cytosol (Colin *et al*, 2018; Inoue *et al*, 2019). Together with evidence revealing that many diffusion barriers are composed of branched actin networks (Lin *et al*, 2013b), it is plausible that branched actin networks are more important than unbranched actin in molecular diffusion.

Recently, the discovery of phase-separation mechanisms in cells has provided new insights into how non-membrane-bound components assemble and maintain their structures (Zwicker *et al*, 2014; Ahn *et al*, 2020). The organelles with phase transition properties generate a gel-like microenvironment in which to concentrate centrosomal molecules locally and to separate this compartment physically from the cytosol (Rale *et al*, 2018). However, whether this centrosomal condensate results in any restrictions on solute mobility is still unclear. Besides branched actin outside centrosomes, pericentriolar matrix also partially interferes with the diffusion of large molecules according to several lines of evidence. The probabilities of large probes trapping to Centrin2-tagged centriolar lumen are less than that to pericentriolar matrix (Table EV1), suggesting that pericentriolar matrix also acts as a size-dependent diffusion barrier to hinder the entry of probes larger than 5.8 nm. Moreover, disruption of branched actin around centrosomes enables the trapping of large probes (6.3 and 7.6 nm) at pericentriolar matrix. However, in the absence of actin-based diffusion barriers, a large probe (7.6 nm) is still difficult to penetrate through pericentriolar matrix to reach Centrin2-tagged centriolar lumen (Fig 4H, right). These results suggest that the pericentriolar matrix may impede the entry of bulky molecules (7.6 nm) to Centrin2-tagged centriolar lumen.

Previous studies demonstrated that centrosomal branched actin acts as a negative regulator of microtubule nucleation (Farina *et al*, 2019; Inoue *et al*, 2019). However, how branched actin at the centrosomes suppresses microtubule nucleation is still unclear. Our results indicated that branched actin prevented large molecules from crossing the centrosome boundary. It is thus plausible that microtubule nucleation would also be physically hindered, although

microtubule elongation, which occurs outside of the centrosomes, was not affected by diffusion barriers.

The approaches developed here have powerful applications beyond probing diffusion mechanisms. Chemically inducible dimerization systems have been widely used to spatiotemporally manipulate cellular architecture and signaling by recruiting proteins of interest (Rs of ≤ 5.8 nm) onto target sites in cells (Lin *et al*, 2013a; Leyton-Puig *et al*, 2016; Fan *et al*, 2017; Hong *et al*, 2018; Lian *et al*, 2020). The current study has established a new system that enables rapid recruitment of proteins of interest onto the centriolar lumen, pericentriolar matrix, or centriolar satellites within seconds. It offers a feasible way to spatiotemporally manipulate molecular signaling at three different centrosomal sub-compartments. This approach should allow us to address previously intractable questions in centrosome biology, a discipline that has a strong translational link to a variety of centrosome-related diseases.

Materials and Methods

DNA constructs

YFP-FKBP, YFP-FKBP-Grp1, YFP-FKBP-Luciferase, YFP-FKBP- Δ N β -Gal, YFP-FKBP- β -Gal, and Lyn-CFP-FRB were generated previously (Lin *et al*, 2013a; Hong *et al*, 2018; Liu *et al*, 2022). For generating CEP120C-GFP, we used the pcDNA4-CEP120-myc (Tsai *et al*, 2019) as a template to amplify C-terminus of CEP120 (a.a. 416–986) and subcloned it into pEGFP-C1 backbone (BD Biosciences Clontech). GFP-Centrin2, GFP-CEP170C1, PCM1F2-GFP, GFP-pericentrin, EB1-mNeon, and YFP-PSD95-FKBP were gifts from Dr. Takanari Inoue's lab. H2B-RFP was a gift from Dr. Lily Hui-Ching Wang. Using YFP-FKBP- β -Gal and YFP-FKBP- Δ N β -Gal as templates, YFP-FKBP- β -Gals and YFP-FKBP- β -Gals, which had a.a. 439–579 and a.a. 340–678 of β -Gal deleted, respectively, were generated by NEBuilder HiFi DNA assembly kit (New England Biolabs). PACT, the c-terminus of pericentrin (a.a. 3,113–3,336), was amplified from GFP-pericentrin, and subclone to pEGFP-C1 (BD biosciences Clontech) or Ce3-FRB vectors (Hong *et al*, 2018). PCM1F2 fragment was digested by restriction enzymes, NheI and AgeI (New England Biolabs) from PCM1F2-GFP, and subcloned to Ce3-FRB vector. Full-length GCP4 and truncated GCP4, which had a.a. 350–666 deleted (GCP4 Δ C), were obtained from the GCP4 cDNA clone (Clone ID: 2821891; PerkinElmer) and subclone to pEGFP-C1 backbone (BD Biosciences Clontech). The sequences of all DNA constructs were confirmed.

Cell culture, transfection, and chemicals

U2Os, HeLa, and 293 T cells (ATCC) were maintained at 37°C in 5% CO₂ in DMEM (Corning) supplemented with 10% fetal bovine serum (Gibco), penicillin, and streptomycin (Corning). Twenty-four hours before live-cell imaging or drug treatment, plasmid DNA transfection was performed with the LT-X (Invitrogen) or TransIT-LT1 transfection reagent (Mirus). Transfected cells were plated on poly-D-lysine (Sigma-Aldrich)-coated borosilicate cover glass (Paul Marienfeld) in six-well culture plates (Sigma-Aldrich). Latrunculin A (Toronto Research Chemicals, J210700; Stock concentration, 2 mM), CK666 (Sigma-Aldrich, M1404; Stock concentration, 0.4 M), rapamycin (LC Laboratories, R-5000; Stock concentration, 100 μ M),

thymidine (Sigma-Aldrich, 50–89-5; Stock concentration, 200 mM), RO3306 (Sigma-Aldrich, 872573-93-8, Stock concentration, 5 mg/ml), and Nocodazole (Sigma-Aldrich, M1404; Stock concentration, 10 mM) were used in the study.

Size exclusion chromatography

A 293 T cells expressing YFP-PSD95-FKBP, YFP-FKBP- β -Gals or YFP-FKBP- β -Galm were lysed by lysis buffer [25 mM Tris (pH7.5), 250 mM NaCl, 1% Triton X-100] and clarified by centrifugation at 14,000 g for 15 min. The supernatant was passed through a 0.22 μ m spin centrifuge filter (Corning) prior to a Superdex 200 Increase 10/300 GL column (GE Healthcare Life Sciences), which was connected to a NGC Chromatography System (Bio-Rad). Soluble proteins were eluted in 30 mM Tris pH7.5, 150 mM NaCl, and 1 mM DTT. The density of YFP-PSD95-FKBP, YFP-FKBP- β -Gals, and YFP-FKBP- β -Galm in each fraction was analyzed by western blotting.

Cell synchronization

HeLa cells were transfected with YFP-FKBP-tagged diffusion probes and PACT-Ce3-FRB plasmids using Fugene HD transfection reagent (Promega) 20–24 h before synchronization. After transfection, cells were incubated with 2 mM thymidine (Sigma) in supplemented DMEM (Corning) for 16–18 h to arrest cells at G1/S phase, followed by 12 h of 2.5 μ g/ml RO3306 (Sigma) incubation in medium to block the cells at G2/M phase. To enrich the population of anaphase cells, cells were washed and released to RO3306-free medium for 45–60 min before imaging (Appendix Fig S10A–C).

Image acquisition

Live-cell imaging was carried out with a Nikon T1 inverted fluorescence microscope with a 60 \times or 100 \times oil objective (Nikon), DS-Qi2 CMOS camera (Nikon), and 37 $^{\circ}$ C, 5% CO₂ heated stage (Live Cell Instrument). Images with multiple z-stacks were processed with Huygens Deconvolution software (Scientific Volume Imaging). Image analysis and the maximum intensity projections of images were generated with Nikon Elements AR software.

Fluorescence recovery after photobleaching assay

U2Os cells transfected with the indicated constructs (GFP-Centrin2, CEP120C-GFP, GFP-CEP170C1, PCMF2-GFP, PACT-GFP, or GCP4-GFP) were imaged every 10 s for 10 min on a confocal laser scanning microscope (Zeiss LSM780). The centrosomal regions of cells expressing the indicated constructs were photobleached and allowed to recover for 300 s. The time-lapse background-subtracted fluorescence intensity for GFP was quantified with Nikon Elements AR software.

Measurement of the kinetics of soluble proteins translocating onto centrosomes

U2Os cells were transfected with the indicated constructs as described above. Cells transfected with YFP-FKBP-tagged diffusion probes and Ce3-FRB-tagged CTSs were imaged every 5 s for 4 min

on a Nikon T1 inverted fluorescence microscope with a 60 \times oil objective (Nikon), DS-Qi2 CMOS camera, and 37 $^{\circ}$ C, 5% CO₂ heated stage. We added 100 nM rapamycin (LC Laboratories) during imaging. Time-lapse images were processed by Huygens Deconvolution software. The intensity of YFP-FKBP-tagged proteins at centrosomes upon rapamycin treatment was measured by Nikon Elements AR software.

Immunofluorescence staining

Cells were plated on poly-D-lysine-coated borosilicate glass Lab-Tek eight-well chambers (Thermo Scientific). For microtubule immunofluorescence labeling, cells were fixed for 15 min at room temperature in 4% paraformaldehyde (Electron Microscopy Sciences). Fixed samples were permeabilized with 0.1% Triton X-100 (Sigma-Aldrich) in phosphate-buffered saline (PBS) for 40 min. Cells were gently rinsed before being incubated in blocking solution (2% bovine serum albumin in PBS) for 30 min at room temperature. Primary antibodies against α -tubulin (1:1,000 dilution; T6199, Sigma-Aldrich), glutamylated tubulin (1:100 dilution; AG-20B-0020-C100, Adipogen), Pericentrin (1:1,000 dilution, ab220784, Abcam), CEP290 (1:500 dilution, ab84870, Abcam), γ -tubulin (1:500 dilution; Sigma-Aldrich, T6557), or PCM1 (1:500 dilution; Proteintech, 19856-1-AP) diluted in blocking solution, were used to stain the cells for 1 h at room temperature. Secondary antibodies diluted in blocking solution (1:1,000 dilution) were incubated with cells for 1 h at room temperature followed by a gentle rinse with PBS. For immunofluorescence labeling of actin filaments, cells transfected with PACT-Ce3-FRB were seeded on poly-D-lysine-coated borosilicate glass Lab-Tek eight-well chambers. Cells were rinsed with pre-warmed PBS before being incubated in 4% paraformaldehyde (Electron Microscopy Sciences) dissolved in cytoskeleton-preserving buffer (80 mM PIPES, pH 6.8; 5 mM EGTA; 2 mM MgCl₂; Leyton-Puig *et al.*, 2016). Cells were permeabilized with 0.5% Triton X-100 (in PBS) followed by Phalloidin 594 (1:330 dilution in PBS; A12381, Invitrogen) staining for 30 min at room temperature.

Tracking microtubule growth

U2Os cells were transfected with EB1-mNeon and seeded on poly-D-lysine-coated borosilicate cover glass in six-well culture plates (Sigma-Aldrich) 24 h prior to imaging. Live-cell imaging was acquired using a 5-s interval over a duration of 5 min and 3 z-stacks. Images were processed with Huygens Deconvolution software and rolling ball correction (Nikon NIS Elements) before being analyzed with ImageJ (Fiji) TrackMate.

Western blot

A 293 T cells were transfected with the YFP-FKBP-tagged probes. 48 h after transfection, cells were lysed using RIPA lysis buffer [Tris-HCl 50 mM, EGTA 20 mM, NaCl 9%, Triton X-100 1%, Roche complete protease inhibitor cocktail tablet (Roche, 04719964001)]. The post-nucleus lysates were analyzed by SDS-PAGE, followed by immunoblotting with anti-Venus antibody (1:1,000, MyBioSource, MBS448126) and horseradish peroxidase-conjugated anti-Goat antibody. The blotting results were visualized by Amersham™ ECL

Select™ (FE Healthcare, RPN2235) and imaged by iBright™ FL1500 Instrument (Thermo Scientific).

Statistical analysis

Statistical analysis was performed with an unpaired two-tailed Student's *t*-test. An *F*-test was used to determine whether variances were equal or not. $P < 0.05$ indicates a significant difference. $P < 0.01$ indicates a highly significant difference.

Data availability

This study includes no data deposited in external repositories.

Expanded View for this article is available [online](#).

Acknowledgments

The original pilot study was conducted by Y.C.L. in Dr. Takanari Inoue's lab (Johns Hopkins University). This study was supported by the National Science and Technology Council, Taiwan (111-2636-B-007-009 to Y.C.L., 109-2311-B-001-020-MY3 to K.C.H., 107-2113-M-007-015 to L.W.Y., and 111-2311-B-007-009 to H.C.C.), National Tsing Hua University (grant number 111Q2713E1 to Y.C.L.), and Academia Sinica (CDA-106-L02 to K.C.H.).

Author contributions

Hsuan Cheng: Data curation; formal analysis; investigation; methodology; writing — original draft; writing — review and editing. **Yu-Lin Kao:** Data curation; formal analysis; investigation; writing — original draft. **Ting Chen:** Investigation; methodology. **Lohitaksh Sharma:** Data curation; software; methodology; writing — original draft. **Wen-Ting Yang:** Data curation; investigation. **Yi-Chien Chuang:** Data curation; formal analysis; investigation. **Shih-Han Huang:** Data curation; investigation. **Hong-Rui Lin:** Formal analysis. **Yao-Shen Huang:** Data curation; investigation. **Ching-Lin Kao:** Writing — original draft. **Lee-Wei Yang:** Supervision. **Rachel Bearon:** Supervision. **Hui-Chun Cheng:** Supervision. **Kuo-Chiang Hsia:** Resources. **Yu-Chun Lin:** Conceptualization; formal analysis; supervision; funding acquisition; validation; investigation; methodology; writing — original draft; project administration; writing — review and editing.

Disclosure and competing interests statement

The authors declare that they have no conflict of interest.

References

- Abal M, Keryer G, Bornens M (2005) Centrioles resist forces applied on centrosomes during G2/M transition. *Biol Cell* 97: 425–434
- Ahn JI, Park JE, Meng L, Zhang L, Kim TS, Kruhlak MJ, Kim BY, Lee KS (2020) Phase separation of the Cep63•Cep152 complex underlies the formation of dynamic supramolecular self-assemblies at human centrosomes. *Cell Cycle* 19: 3437–3457
- Aridor M, Hannah LA (2000) Traffic jam: a compendium of human diseases that affect intracellular transport processes. *Traffic* 1: 836–851
- Ataei F, Hosseinkhani S, Khajeh K (2009) Luciferase protection against proteolytic degradation: a key for improving signal in nano-system biology. *J Biotechnol* 144: 83–88
- Balasanyan V, Watanabe K, Dempsey WP, Lewis TL, Trinh LA, Arnold DB (2017) Structure and function of an actin-based filter in the proximal axon. *Cell Rep* 21: 2696–2705
- Banaszynski LA, Liu CW, Wandless TJ (2005) Characterization of the FKBP-rapamycin-FRB ternary complex. *J Am Chem Soc* 127: 4715–4721
- Bettencourt-Dias M, Glover DM (2007) Centrosome biogenesis and function: centrosomes brings new understanding. *Nat Rev Mol Cell Biol* 8: 451–463
- Breslow DK, Koslover EF, Seydel F, Spakowitz AJ, Nachury MV (2013) An *in vitro* assay for entry into cilia reveals unique properties of the soluble diffusion barrier. *J Cell Biol* 203: 129–147
- Buffington S, Rasband M (2011) The axon initial segment in nervous system disease and injury. *Eur J Neurosci* 34: 1609–1619
- Burke TA, Christensen JR, Barone E, Suarez C, Sirotkin V, Kovar DR (2014) Homeostatic actin cytoskeleton networks are regulated by assembly factor competition for monomers. *Curr Biol* 24: 579–585
- Caudron F, Barral Y (2009) Septins and the lateral compartmentalization of eukaryotic membranes. *Dev Cell* 16: 493–506
- Chavali PL, Pu M, Gergely F, Gergely F (2014) Small organelle, big responsibility: the role of centrosomes in development and disease. *Philos Trans R Soc Lond B Biol Sci* 369: 20130468
- Colin A, Singaravelu P, Théry M, Blanchoin L, Gueroui Z (2018) Actin-network architecture regulates microtubule dynamics. *Curr Biol* 28: 2647–2656.e4
- Cronshaw JM, Matunis MJ (2004) The nuclear pore complex: disease associations and functional correlations. *Trends Endocrinol Metab* 15: 34–39
- DeRose R, Miyamoto T, Inoue T (2013) Manipulating signaling at will: chemically-inducible dimerization (CID) techniques resolve problems in cell biology. *Pflugers Arch* 465: 409–417
- Dertinger T, Pacheco V, von der Hocht I, Hartmann R, Gregor I, Enderlein J (2007) Two-focus fluorescence correlation spectroscopy: a new tool for accurate and absolute diffusion measurements. *Chemphyschem* 8: 433–443
- Digman MA, Gratton E (2009) Imaging barriers to diffusion by pair correlation functions. *Biophys J* 97: 665–673
- Elowitz MB, Surette MG, Wolf P, Stock J, Leibler S (1997) Photoactivation turns green fluorescent protein red. *Curr Biol* 7: 809–812
- Fan CH, Huang YS, Huang WE, Lee AA, Ho SY, Kao YL, Wang CL, Lian YL, Ueno T, Andrew Wang TS et al (2017) Manipulating cellular activities using an ultrasound-chemical hybrid tool. *ACS Synth Biol* 6: 2021–2027
- Farache D, Jauneau A, Chemin C, Chartrain M, Rémy MH, Merdes A, Haren L (2016) Functional analysis of δ -tubulin complex proteins indicates specific lateral association via their N-terminal domains. *J Biol Chem* 291: 23112–23125
- Farina F, Gaillard J, Guérin C, Couté Y, Sillibourne J, Blanchoin L, Théry M (2016) The centrosome is an actin-organizing centre. *Nat Cell Biol* 18: 65–75
- Farina F, Ramkumar N, Brown L, Eweis DS, Anstatt J, Waring T, Bithell J, Scita G, Thery M, Blanchoin L et al (2019) Local actin nucleation tunes centrosomal microtubule nucleation during passage through mitosis. *EMBO J* 38: e99843
- Fujiwara I, Zweifel ME, Courtemanche N, Pollard TD (2018) Latrunculin A accelerates actin filament depolymerization in addition to sequestering actin monomers. *Curr Biol* 28: 3183–3192.e2

- Haren L, Farache D, Emorine L, Merdes A (2020) A stable sub-complex between GCP4, GCP5 and GCP6 promotes the assembly of tubulin ring complexes. *J Cell Sci* 133: jcs244368
- Hellriegel C, Gratton E (2009) Real-time multi-parameter spectroscopy and localization in three-dimensional single-particle tracking. *J R Soc Interface* 6: S3–S14
- Hetrick B, Han MS, Helgeson LA, Nolen BJ (2014) Small molecules CK-666 and CK-869 inhibit Arp2/3 complex by blocking an activating conformational change. *Chem Biol* 20: 701–712
- Higgs HN, Peterson KJ (2005) The forkhead-associated domain protein Cep170 interacts with Polo-like kinase 1 and serves as a marker for mature centrioles. *Mol Biol Cell* 16: 1095–1107
- Hoelz A, Debler EW, Blobel G (2011) The structure of the nuclear pore complex. *Annu Rev Biochem* 80: 613–643
- Hong SR, Wang CL, Huang YS, Chang YC, Pusapati GV, Lin CY, Hsu N, Cheng HC, Chiang YC, Huang WE et al (2018) Spatiotemporal manipulation of ciliary glutamylation reveals its roles in intraciliary trafficking and Hedgehog signaling. *Nat Commun* 9: 1732
- Inoue D, Obino D, Pineau J, Farina F, Gaillard J, Guerin C, Blanchoin L, Lennon-Duménil A, Théry M (2019) Actin filaments regulate microtubule growth at the centrosome. *EMBO J* 38: e99630
- Johnston JA, Ward CL, Kopito RR (1998) Aggresomes: a cellular response to misfolded proteins. *J Cell Biol* 143: 1883–1898
- Kopito RR (2000) Aggresomes, inclusion bodies and protein aggregation. *Trends Cell Biol* 10: 524–530
- Leyton-Puig D, Kedziora KM, Isogai T, VanBroek B, Jalink K, Innocenti M (2016) PFA fixation enables artifact-free super-resolution imaging of the actin cytoskeleton and associated proteins. *Biol Open* 5: 1001–1009
- Lian YL, Chen KW, Chou YT, Ke TL, Chen BC, Lin YC, Chen L (2020) PIP3 depletion rescues myoblast fusion defects in human rhabdomyosarcoma cells. *J Cell Sci* 133: jcs.240325
- Lin YC, Niewiadomski P, Lin B, Nakamura H, Phua SC, Jiao J, Levchenko A, Inoue T, Rohatgi R, Inoue T (2013a) Chemically inducible diffusion trap at cilia reveals molecular sieve-like barrier. *Nat Chem Biol* 9: 437–443
- Lin YC, Phua SC, Lin B, Inoue T (2013b) Visualizing molecular diffusion through passive permeability barriers in cells: conventional and novel approaches. *Curr Opin Chem Biol* 17: 663–671
- Liu GY, Chen SC, Lee GH, Shaiv K, Chen PY, Cheng H, Hong SR, Yang WT, Huang SH, Chang YC et al (2022) Precise control of microtubule disassembly in living cells. *EMBO J* 41: e110472
- Lukyanov K, Chudakov D, Lukyanov S, Verkhusha VV (2005) Innovation: photoactivatable fluorescent proteins. *Nat Rev Mol Cell Biol* 6: 885–890
- Mahen R, Venkitaraman AR (2012) Pattern formation in centrosome assembly. *Curr Opin Cell Biol* 24: 14–23
- Mahjoub MR, Xie Z, Stearns T (2010) Cep120 is asymmetrically localized to the daughter centriole and is essential for centriole assembly. *J Cell Biol* 191: 331–346
- Michalet X, Berglund AJ (2012) Optimal diffusion coefficient estimation in single-particle tracking. *Phys Rev E Stat Nonlin Soft Matter Phys* 85: 61916
- Musa H, Orton C, Morrison EE, Peckham M (2003) Microtubule assembly in cultured myoblasts and myotubes following nocodazole induced microtubule depolymerisation. *J Muscle Res Cell Motil* 24: 301–308
- Nachury MV, Seeley ES, Jin H (2010) Trafficking to the ciliary membrane: how to get across the periciliary diffusion barrier? *Annu Rev Cell Dev Biol* 26: 59–87
- Nolen BJ, Tomasevic N, Russell A, Pierce DW, Jia Z, McCormick CD, Hartman J, Sakowicz R, Pollard TD (2009) Characterization of two classes of small molecule inhibitors of Arp2/3 complex. *Nature* 460: 1031–1034
- Obino D, Farina F, Malbec O, Sáez PJ, Maurin M, Gaillard J, Dingli F, Loew D, Gautreau A, Yuseff MI et al (2016) Actin nucleation at the centrosome controls lymphocyte polarity. *Nat Commun* 7: 10969
- Oegema K, Wiese C, Martin OC, Milligan RA, Iwamatsu A, Mitchison TJ, Zheng Y (1999) Characterization of two related *Drosophila* γ -tubulin complexes that differ in their ability to nucleate microtubules. *J Cell Biol* 144: 721–733
- Paoletti A, Moudjou M, Paintrand M, Salisbury JL, Bornens M (1996) Most of centrin in animal cells is not centrosome-associated and centrosomal centrin is confined to the distal lumen of centrioles. *J Cell Sci* 109: 3089–3102
- Pihan GA (2013) Centrosome dysfunction contributes to chromosome instability, chromoanagenesis, and genome reprogramming in cancer. *Front Oncol* 3: 277
- Potma EO, DeBoeij WP, Bosgraaf L, Roelofs J, van Haastert PJ, Wiersma DA (2001) Reduced protein diffusion rate by cytoskeleton in vegetative and polarized *Dictyostelium* cells. *Biophys J* 81: 2010–2019
- Rale MJ, Kadzik RS, Petry S (2018) Phase transitioning the centrosome into a microtubule nucleator. *Biochemistry* 57: 30–37
- Ries J, Schwille P (2012) Fluorescence correlation spectroscopy. *Bioessays* 34: 361–368
- Roll-Mecak A (2019) Auditory and vestibular research. *Curr Opin Cell Biol* 56: 102–108
- Rout MP, Field MC (2017) The evolution of organellar coat complexes and organization of the eukaryotic cell. *Annu Rev Biochem* 86: 637–657
- Schaeffer C, Creatore A, Rampoldi L (2014) Protein trafficking defects in inherited kidney diseases. *Nephrol Dial Transplant* 29: iv33–iv44
- Song AH, Wang D, Chen G, Li Y, Luo J, Duan S, Poo MM (2009) A selective filter for cytoplasmic transport at the axon initial segment. *Cell* 136: 1148–1160
- Strzyz P (2016) Cytoskeleton: a new face of the centrosome. *Nat Rev Mol Cell Biol* 17: 66–67
- Tanahasi N, Tsurumi C, Tamura T, Tanaka K (1993) Molecular structures of 20 S and 26 S proteasomes. *Enzyme Protein* 47: 241–251
- Tang N, Marshall WF (2012) Centrosome positioning in vertebrate development. *J Cell Sci* 125: 4951–4961
- Thawani A, Petry S (2021) Molecular insight into how γ -TuRC makes microtubules. *J Cell Sci* 134: jcs245464
- Tsai JJ, Hsu WB, Liu JH, Chang CW, Tang TK (2019) CEP120 interacts with C2CD3 and Talpid3 and is required for centriole appendage assembly and ciliogenesis. *Sci Rep* 9: 6037
- Turner-Bridger B, Jakobs M, Muresan L, Wong H, Franze K, Harris WA, Holt CE (2018) Single-molecule analysis of endogenous β -actin mRNA trafficking reveals a mechanism for compartmentalized mRNA localization in axons. *Proc Natl Acad Sci U S A* 115: e9697–e9706
- Venturoli D, Rippe B (2005) Ficoll and dextran vs globular proteins as probes for testing glomerular permselectivity: effects of molecular size, shape, charge, and deformability. *Am J Physiol Renal Physiol* 288: 605–613
- Wang G, Chen Q, Zhang X, Zhang B, Zhuo X, Liu J, Jiang Q, Zhang C (2013) PCMI recruits Plk1 to the pericentriolar matrix to promote primary cilia disassembly before mitotic entry. *J Cell Sci* 126: 1355–1365
- Westlake CJ, Baye LM, Nachury MV, Wright KJ, Ervin KE, Phu L, Chalouni C, Beck JS, Kirkpatrick DS, Slusarski DC et al (2011) Primary cilia membrane assembly is initiated by Rab11 and transport protein particle II (TRAPP1) complex-dependent trafficking of Rabin8 to the centrosome. *Proc Natl Acad Sci U S A* 108: 2759–2764
- Wu J, Akhmanova A (2017) Microtubule-organizing centers. *Annu Rev Cell Dev Biol* 33: 51–75

- Wu CT, Chen HY, Tang TK (2018) Myosin-Va is required for preciliary vesicle transportation to the mother centriole during ciliogenesis. *Nat Cell Biol* 20: 175–185
- Yang Q, Zhang XF, Pollard TD, Forscher P (2012) Arp2/3 complex-dependent actin networks constrain myosin II function in driving retrograde actin flow. *J Cell Biol* 197: 939–956
- Zheng C, Petralia RS, Wang Y, Kachar B (2011) Fluorescence recovery after photobleaching (FRAP) of fluorescence tagged proteins in dendritic spines of cultured hippocampal neurons. *J Vis Exp* 16: 2568

- Zwicker D, Decker M, Jaensch S, Hyman AA, Jülicher F (2014) Centrosomes are autocatalytic droplets of pericentriolar material organized by centrioles. *Proc Natl Acad Sci U S A* 111: e2636–e2645



License: This is an open access article under the terms of the [Creative Commons Attribution-NonCommercial-NoDerivs](#) License, which permits use and distribution in any medium, provided the original work is properly cited, the use is non-commercial and no modifications or adaptations are made.